Anomalous continuous-time random-walk spectral diffusion in coherent third-order optical response

František Šanda and Shaul Mukamel*
Department of Chemistry, University of California, Irvine, California 92697, USA
(Received 1 August 2005; published 17 January 2006)

Recursive relations are derived for nonlinear optical response functions of a two-level chromophore with stochastic frequency fluctuations described by a continuous-time random walk. Stationary ensembles are constructed and signatures of anomalous relaxation in the photon echo signal are discussed for a two state jump modulation with a power law waiting time density function $\psi(t) \sim t^{-\alpha-1}$. Stretched exponential decay of the photon echo signal is predicted for $0<\alpha<1$ and power law asymptotics for $1<\alpha<2$.

DOI: 10.1103/PhysRevE.73.011103 PACS number(s): 05.40.Fb, 02.50.−r, 42.65.−k

I. INTRODUCTION

Spectral line broadening reveals the dynamics of the environment as it modulates the frequency of a chromophore. The stochastic Liouville equations (SLE) proposed by Kubo and Anderson [1–3] describe the absorption line shapes of a two level chromophore undergoing a Markovian stochastic frequency modulation. Stochastic models may be derived from microscopic models of fluctuations. For example, the Uhlenbeck-Ornstein process [4,5] is obtained from the spin-boson model [6] in the limit of overdamped oscillator spectral density and at infinite temperature. Memory effects are commonly modelled by using various types of master equations [7–12].

Multipoint correlation functions obtained from studies of single molecules [13,14] and from nonlinear spectroscopy [15] are fundamental characteristics of dynamical models which carry more information than two-point quantities [16]. The SLE are time-local Markovian equations whose Green functions may be used to calculate multipoint quantities. In the absence of a Markovian description this modeling is much more complex [17,18].

Stochastic trajectories of single protein molecules and quantum dots show stretched-exponential $C(t) \propto \exp(-t^{\alpha})$ or power-law $C(t) \propto t^{-\alpha}$ two-point correlation functions of fluorescence intensities [19–24]. Continuous time random walks (CTRW) [25–31] generalize ordinary random walks by introducing a waiting time probability density function (WTDF) $\psi(t)$ for stochastic jumps, and provide a convenient formalism for describing long time memory effects. Broad waiting time distributions result in long-tailed correlation functions of the stochastic variable [31–33]. Broad distributions of step lengths (Lévy flights) have been studied as well [33–36] but will not be considered here. The asymptotic properties of random walks with these broad distributions were studied extensively and related to Lévy stable distributions [36–41].

By assuming that all particles made a jump at the time origin we obtain a nonstationary process. This ensemble never becomes equilibrated for WTDF with infinite mean $\bar{t}=\int_0^{\infty} t\psi(t)dt$; this effect is known as aging [42].

To describe a stationary process, we must assume a special WTDF for the first jump. This can only be established for WTDF with a finite mean $\bar{t}$ [43], e.g., $\psi(t) \sim 1/t^{1+\alpha}$, with $\alpha>1$. For $1>\alpha>0$ a step function [44] or an exponential [45] long time cutoff were introduced to keep the first moment finite. This was applied to two state CTRW model of fluorescence on/off time statistics or absorption lineshape, respectively.

The application of CTRW to spectral diffusion in lineshapes and nonlinear spectroscopy requires its extension to describe optical coherence. Recently, the two state jump (TSJ) model with CTRW modulation of bath fluctuations was applied to absorption lineshapes (linear response) [45]. This is a two point correlation function that depends on phase fluctuations which cause the decay of coherence (dephasing). The model was further extended to include multistate bath fluctuations [46–48].

In this paper we calculate multipoint correlation functions by introducing auxiliary quantities: densities of jumps [18]. This strategy goes back to the early days of the CTRW model [25]. An alternative procedure is to add a variable describing the time from the last jump [46]. The WTDF for a jump are then interpreted as Markovian rates for transitions from the state associated with a particular time from the last jump. The CTRW is thus embedded into a higher-dimensional Markovian process, and multitime correlation functions may be calculated using the SLE. This approach which resembles the age-dependent master equations ADME [49,50] has not been implemented for simulations of multipoint quantities.

In Sec. II we consider a two level system with a fluctuating frequency and calculate the lineshape for the TSJ CTRW model of frequency modulation. Stationary ensembles for WTDF with power-law long time decays are introduced to study the signatures of anomalous relaxation in lineshapes. The algorithm for calculating multipoint Liouville space correlation functions with CTRW fluctuations, which is the central result of this work, is presented in Sec. III. Signatures of anomalous diffusion in the photon echo technique are then predicted in Sec. IV and discussed in Sec. V.

II. SPECTRAL LINE SHAPES; LINEAR RESPONSE

We consider a two-level system with a ground $|g\rangle$ and an excited state $|e\rangle$, transition frequency ω_{eg}, and dipole mo-

*Email address: smukamel@uci.edu

ment μ interacting with an optical field E with frequency ω and described by the Hamiltonian

$$\hat{H}_S = |e\rangle[\omega_{eg} + \delta\omega_{eg}(t)]\langle e| - E\mu[|g\rangle\langle e|\exp(-i\omega t) + |e\rangle\langle g|\exp(i\omega t)]. \quad (1)$$

$\delta\omega_{eg}(t)$ are frequency fluctuations caused by interaction with the environment.

The absorption line shape is given by

$$I(\omega) \equiv \frac{1}{\pi}\,\mathrm{Re}\int_0^\infty dt e^{i(\omega-\omega_{eg})t}S(t), \quad (2)$$

where

$$S(t) \equiv \left\langle \exp\left(-i\int_0^t \delta\omega_{eg}(\tau)d\tau\right)\right\rangle \quad (3)$$

is the linear response function [1,51]. The line shape may be expressed using the Laplace transform of the response function $\tilde{S}(s) \equiv \int_0^\infty e^{-st}S(t)dt$

$$I(\omega+\omega_{eg}) = \frac{1}{\pi}\,\mathrm{Re}\,\tilde{S}(-i\omega). \quad (4)$$

Equation (3) can be calculated by solving the differential equation for the fluctuating optical coherence

$$\frac{d\rho_{eg}(t)}{dt} = -i\delta\omega_{eg}(t)\rho_{eg}(t) \quad (5)$$

with $\rho_{eg}(0)=1$. We then have $S(t)=\langle\rho_{eg}(t)\rangle$.

In the TSJ model [1–3] the frequency fluctuations are caused by coupling the chromophore to a two-level bath. $\delta\omega_{eg}$ can then assume the values $-\omega_0$ and ω_0, when the bath is in the state a and b, respectively. The Liouville operator is represented in a,b space as

$$\hat{L} = \begin{pmatrix} -i\omega_0 & 0 \\ 0 & i\omega_0 \end{pmatrix}. \quad (6)$$

The stochastic dynamics of the bath is described as a CTRW [31]. The survival probability $\phi(t)$ that no jump had occurred for time t is connected with the waiting time density function $\psi(t)$ by

$$\phi(t) = \int_t^\infty \psi(t')dt',$$

or in Laplace space:

$$\tilde{\phi}(s) = \frac{1-\tilde{\psi}(s)}{s}. \quad (7)$$

We define the matrix of jump rates in the a,b space:

$$\hat{\Psi}(t) = \begin{pmatrix} 0 & \psi(t) \\ \psi(t) & 0 \end{pmatrix} \quad (8)$$

and the corresponding matrix of survival probabilities

$$\hat{\Phi}(t) = \begin{pmatrix} \phi(t) & 0 \\ 0 & \phi(t) \end{pmatrix}. \quad (9)$$

The first jump is special, since its WTDF ψ' depends on the nature of the initial ensemble. This is particulary important when $\psi(t)$ has long algebraic tails and the memory of the first jump may persist for long times. If the moments of ψ are finite the memory of the first jump is erased and does not affect the long-time behavior.

Assuming that the CTRW starts at $t=0$ we can set $\psi(t)=\psi'(t)$ and obtain a nonstationary ensemble. For the ensemble to be stationary we must have [43,52]

$$\psi'(t) = \phi(t)/\bar{t} \quad (10)$$

where $\bar{t}$ is the mean waiting time (first moment of ψ):

$$\bar{t} = \int_0^\infty \tau\psi(\tau)d\tau = -\left.\frac{d\tilde{\psi}(s)}{ds}\right|_{s=0}.$$

A stationary CTRW is only possible provided the WTDF has a finite mean. Equation (10) is a consequence of microscopic reversibility: At equilibrium, we observe the same WTDF for the first jump forward $[\psi'(t)]$ or for the backward evolution. The latter is a product of the survival function $\phi(t)$ and equilibrium density of jumps $1/\bar{t}$.

The Green function solution to Eq. (5) is

$$S(t) = \langle\rho_{eg}(t)\rangle = \langle\hat{G}(t)\rho_{eg}(0)\rangle. \quad (11)$$

For the TSJ model it is represented in the a,b space by a 2×2 matrix, and the response function is obtained by averaging over initial and summing over final states

$$S(t) = \sum_{j,l=a,b} G_{jl}(t)[\rho_{eg}]_l(0). \quad (12)$$

Anomalous relaxation models are characterized by long algebraic tails for WTDF $\psi(t)\propto t^{-(\alpha+1)}$. In Laplace space, the moments of ψ are obtained as

$$\langle t^k\rangle = (-1)^k \left.\frac{d^k\tilde{\psi}(s)}{ds^k}\right|_{s=0}.$$

The kth moment diverge for $k\geqslant\alpha$. The small s behavior is connected to the moments of $\psi(t)$ as $\tilde{\psi}(s)\approx 1-s\bar{t}+s^2\langle t^2\rangle/2+\ldots$.

We have simulated the following three models of spectral diffusion.

(i) Markovian fluctuations (model M)

CTRW is generally a non-Markovian process; knowing the present state of the system is not sufficient to predict its future evolution since it also depends on the distribution of prior jumps (history). An exception is when $\psi(t)=\Lambda e^{-\Lambda t}$ where the bath may be described by ordinary Markovian rate equations and the system-bath dynamics is described by the SLE [1]

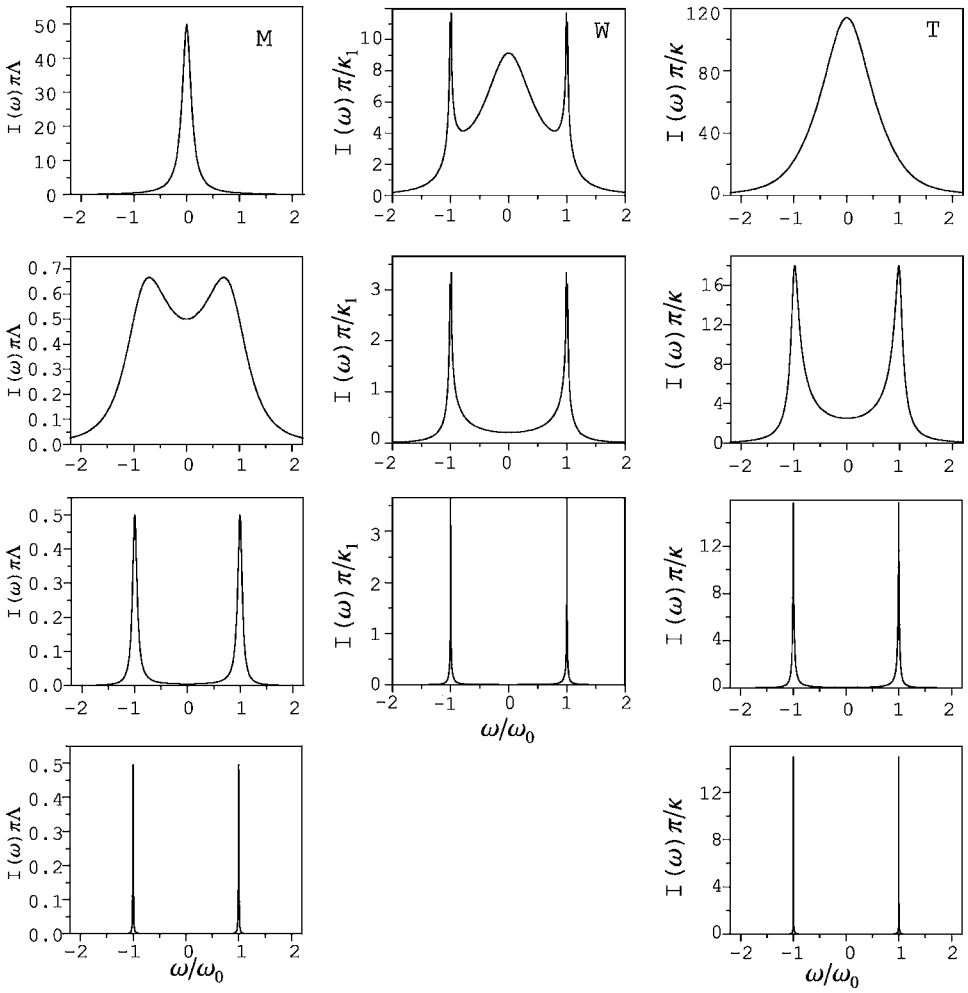

FIG. 1. Absorption line shapes [Eq. (4); $\omega_{eg}=0$], for models M (left column) [Eq. (18)], W (central column) [Eq. (19)], and T (right column) [Eq. (21)]. Parameters interpolate from the fast (top row) to the slow (bottom row) fluctuation regime. Parameters (from top to bottom). M: $\omega_0/\Lambda=0.2$, 2, 20, 200. W: $\alpha=1.5$, $\kappa_1/\kappa_\alpha=1.5$, $\omega_0\kappa_1=0.2$, 2, 20. T: $\alpha=0.5$, $\kappa\lambda=0.01$, $\omega_0\kappa=0.02$, (dash-dotted line) 0.2, 2, 20.

$$\frac{d\rho_{eg}(t)}{dt}=\hat{L}\rho_{eg}(t)+[\hat{\Psi}(0)-\Lambda\hat{1}]\rho_{eg}(t). \tag{13}$$

This is known as the Kubo-Anderson model [1–3] for spectral diffusion.

(ii) Weak anomalous fluctuations (model W)

When $\psi(t)\propto t^{-1-\alpha}$ with $1>\alpha>2$, $\bar{t}$ is finite but $\langle t^2\rangle$ diverges [37,48]. In Laplace space $\psi(s)\sim 1-s+s^\alpha$, $s\to 0$. The central limit theorem does not apply, and broad distributions of waiting times for k steps can persist for $k\to\infty$ [38–40]. We assume [18]

$$\tilde{\psi}_W(s)=\frac{1}{1+\kappa_1 s/[1+(\kappa_\alpha s)^{\alpha-1}]}.$$

By using Eqs. (7) and (10) we have

$$\tilde{\psi}'_W(s)=\frac{1}{1+\kappa_1 s+(\kappa_\alpha s)^{\alpha-1}},\quad \tilde{\phi}'_W(s)=\frac{\kappa_1 s+(\kappa_\alpha s)^{\alpha-1}}{s[1+\kappa_1 s+(\kappa_\alpha s)^{\alpha-1}]}.$$

This implies for long times

$$\psi_W(t)\approx\frac{\kappa_\alpha^{\alpha-1}\kappa_1}{\Gamma(-\alpha)t^{\alpha+1}},\quad \psi'_W(t)\approx\frac{-\kappa_\alpha^{\alpha-1}}{\Gamma(1-\alpha)t^{\alpha}},$$

$$\phi'_W(t)\approx\frac{\kappa_\alpha^{\alpha-1}}{\Gamma(2-\alpha)t^{\alpha-1}}.$$

This asymptotic result applies when $\kappa s\ll 1$, i.e., for $t\gg\kappa_\alpha$ and $\kappa_1 s\ll(\kappa_\alpha)s^{\alpha-1}$, i.e., $t\gg\kappa_1^{1/(2-\alpha)}/\kappa_\alpha^{(\alpha-1)/(2-\alpha)}$.

(iii) Truncated anomalous fluctuations (model T)

For $\psi(t)\propto t^{-1-\alpha}$ with $0>\alpha>1$, all moments of $\psi(t)$ including the first $\bar{t}$ diverge. In Laplace space $\tilde{\psi}(s)\approx 1-(\kappa s)^\alpha$ at $s\to 0$. To construct a stationary ensembles [18,44,45] we add a long-time exponential cutoff. This gives [18]

$$\tilde{\psi}_T(s)=\frac{1+(\kappa\lambda)^\alpha}{1+[\kappa(s+\lambda)]^\alpha},\quad \bar{t}=\frac{\alpha\lambda^{-1}}{1+(\kappa\lambda)^{-\alpha}},$$

$$\tilde{\psi}'_T(s)=\frac{(s+\lambda)^\alpha-\lambda^\alpha}{s\bar{t}[\kappa^{-\alpha}+(s+\lambda)^\alpha]},\quad \phi'_T(s)=\frac{1}{s}-\frac{(s+\lambda)^\alpha-\lambda^\alpha}{s^2\bar{t}[\kappa^{-\alpha}+(s+\lambda)^\alpha]}. \tag{14}$$

It describes the algebraic $\psi(t)\approx(\kappa/t)^{\alpha+1}$ decay at intermediate time scale $\lambda t\ll 1$ with a crossover to exponential $e^{-\lambda t}$ decay at long times. For $\kappa\lambda\ll 1$, the long time asymptotics $t/\kappa\to\infty$ are

$$\psi_T(t)\approx\frac{e^{-\lambda t}\kappa^\alpha}{\Gamma(1-\alpha)t^{1+\alpha}},\quad \psi'_T(t)\approx\frac{e^{-\lambda t}}{\lambda^\alpha\Gamma(1-\alpha)t^{1+\alpha}},$$

$$\phi_T'(t) \approx \frac{e^{-\lambda t}}{\Gamma(1-\alpha)(\lambda t)^{1+\alpha}}.$$

We have calculated the linear response function using the approach of [45]. Our notation follows the non-Markovian SLE introduced in [46]. We define the auxiliary matrix $\hat{R}(t_1)$ which describes the contribution to the Green function $\hat{G}(t_1)$ from a path whose last jump occurred precisely at time t_1. $\hat{R}$ is given by [45,46]

$$\hat{R}(t_1) = \hat{\Psi}'(t_1)\exp[\hat{L}t_1] + \int_0^{t_1} dt_1' \hat{\Psi}(t_1 - t_1')\exp[\hat{L}(t_1 - t_1')]R(t_1'). \quad (15)$$

The Green function is finally given by

$$\hat{G}(t_1) = \hat{\Phi}'(t_1)\exp[\hat{L}(t_1)] + \int_0^{t_1} dt_1' \hat{\Phi}(t_1 - \tau_1)\exp[\hat{L}(t_1 - t_1')]\hat{R}(t_1'). \quad (16)$$

Using the initial equilibrium distribution $\rho_a(0)=\rho_b(0)=0.5$, for a stationary ensemble we substitute Eqs. (10) and Eq. (12) in Eq. (16) and obtain in Laplace space (see Appendix A) [45]

$$2\tilde{S}(s) = \frac{1}{s+i\omega_0} + \frac{1}{s-i\omega_0} - \frac{[1-\tilde{\psi}(s+i\omega_0)][1-\tilde{\psi}(s-i\omega_0)]}{\bar{t}[1-\tilde{\psi}(s-i\omega_0)\tilde{\psi}(s+i\omega_0)]} \times \left(\frac{1}{s+i\omega_0} - \frac{1}{s-i\omega_0}\right)^2. \quad (17)$$

We now compare the absorption lineshapes for the three models. For model M we get [1]

$$I(\omega+\omega_{eg}) = \frac{2\Lambda\omega_0^2}{\pi[(\omega^2-\omega_0^2)^2 + 4\Lambda^2\omega^2]}. \quad (18)$$

These are plotted in the left column of Fig. 1. From top to bottom they interpolate between the fast fluctuation (motional narrowing, large ω_0/Λ) and the slow fluctuation (static, small ω_0/λ) limits.

The line shape for the W model

$$I(\omega+\omega_{eg}) = \frac{2\omega_0^2}{\pi(\omega_0^2-\omega^2)^2} \times \mathrm{Re}\,\frac{1}{\kappa_1 + \kappa_\alpha^{\alpha-1}[(i\omega_0 - i\omega)^{\alpha-2} + (-i\omega - i\omega_0)^{\alpha-2}] + i(\omega-\omega_0)^{-1} + i(\omega+\omega_0)^{-1}} \quad (19)$$

is displayed in the middle column. The fraction of particles that remained at the initial position is significant (not exponentially small) over all time scales. Consequently the lineshape [Eq. (19)] has peaks at $s=\pm i\omega_0$

$$I(\omega_0+\omega_{eg}) \approx \cos\,\pi(1-\alpha/2)\kappa_\alpha^{\alpha-1}|\omega-\omega_0|^{\alpha-2}/2. \quad (20)$$

The upper panel of Fig. 2 shows the power law divergence as straight lines in log-log plot with slope $\alpha-2$. The peaks at $\omega=\pm\omega_0$ are universal and reflect the asymptotic power law exponent of $\phi'(t)$.

The lineshape for the T model

$$I(\omega+\omega_{eg}) = \frac{2\omega_0^2}{\pi\bar{t}(\omega_0^2-\omega^2)^2}\,\mathrm{Re}\,\frac{1}{1+(\lambda^\alpha+\kappa^{-\alpha})\left[\frac{1}{(\lambda+i(\omega_0-\omega))^\alpha-\lambda^\alpha} + \frac{1}{(\lambda-i(\omega_0+\omega))^\alpha-\lambda^\alpha}\right]} \quad (21)$$

is displayed in the right column of Fig. 1. With decreasing λ the static limit (bottom panel) is approached. The Kubo-Anderson theory is recovered for $\lambda\kappa \gg 1$ or for $\alpha\to 1$. For $\lambda t \gg 1$ the response function [Eq. (21)] decays exponentially, and we have finite absorption at $\pm\omega_0$ peaks eventually diverging in $\lambda\to 0$ limit.

The signatures of power-law decay may be best seen for $\lambda\kappa \ll 1$, where we have two peaks at $\omega=\omega_{eg}\pm\omega_0$, which for $\lambda \ll |\omega-\omega_0| \ll \omega_0, \kappa^{-1}$ behave as $1/(\omega\pm\omega_0)^{2-\alpha}$. This power law is seen in the lower panel of Fig. 2 for $\kappa\lambda = 10^{-6}$.

These results are in qualitative agreement with [45] where the line shape was calculated for a Levy WTDF $\tilde{\psi}(s)=\exp(-(rs)^\alpha)$. In the next section we present multipoint quantities for the same models.

III. RECURSION RELATIONS FOR MULTIPOINT RESPONSE FUNCTIONS

The response functions for nonlinear spectroscopies are given by correlation functions which represent Liouville space pathways ν [15]. The interactions with the electric field divide the time to intervals $t_j \equiv \tau_j - \tau_{j-1}$, during which the density matrix is in a given state $|\nu^{(j)}\rangle$ whose frequency $\omega_\nu^{(j)}$ fluctuates with the state of the bath. The density matrix elements of the two level system [Eq. (1)] are $|ee\rangle$, $|gg\rangle$, $|eg\rangle$, or $|ge\rangle$ with corresponding frequencies 0, 0, ω_{eg} or $-\omega_{eg}$ respectively.

As an example, we consider the following pathway for the third order response (photon echo) $|gg\rangle\to|ge\rangle\to|eg\rangle\to|gg\rangle$ represented by the Feynman diagram in Fig. 3(a). The second and third interaction times coincide $\tau_1=\tau_2$, $t_2=0$ and the

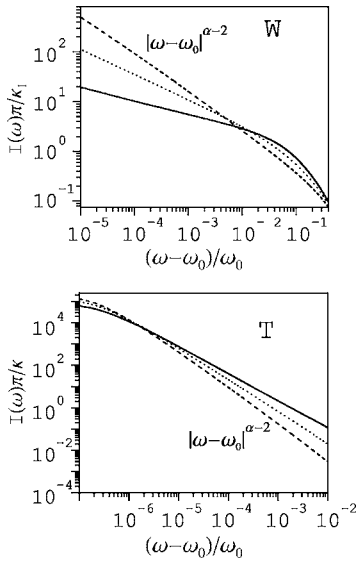

FIG. 2. Upper panel: Absorption line shapes for model W for $\kappa_\alpha/\kappa=2$, $\omega_0\kappa_1=2$, and $\alpha=1.3$ (dashed line), 1.5(dotted line), 1.7 (solid line). Log-log plot for $\omega>\omega_0$ shows the power law $(\omega-\omega_0)^{\alpha-2}$ divergence at peaks $\omega=\pm\omega_0$. Lower panel: Absorption line shape for model T for small $\kappa\lambda=10^{-6}$. The log-log plot shows the power laws $(\omega-\omega_0)^{2-\alpha}$ when κ^{-1}, $\omega_0\gg(\omega-\omega_0)\gg\lambda$ for $\omega_0\kappa=10$ and $\alpha=0.3$ (dashed line), $\alpha=0.5$ (dotted line), $\alpha=0.7$ (solid line).

frequencies during the intervals t_1 (t_3) are $\omega^{(1)}=-\omega_{eg}$ ($\omega^{(3)}=\omega_{eg}$). More generally, we define the nth order response function for the ν pathway

$$S_\nu^{(n)}(t_n,\ldots,t_1)=\langle\rho_\nu\rangle=\left\langle\prod_{j=1}^{n}\exp\left[-i\int_{\tau_{j-1}}^{\tau_j}\delta\omega_\nu^{(j)}(\tau_j)d\tau_j\right]\right\rangle. \tag{22}$$

The generating function ρ_ν is given by the solution of

$$\frac{d\rho_\nu}{dt}=-i\delta\omega_\nu(t)\rho_\nu, \tag{23}$$

where $\delta\omega_\nu(t)=\delta\omega^{(j)}(t)$ for $t\in(\tau_{j-1},\tau_j)$.

In the bath space, $\delta\omega$ is represented by Eq. (6). The Green function is represented in a,b space by a matrix $\hat{G}^{(n)}$ whose jl elements account for contributions to $S^{(n)}$ from paths with fixed initial state l and final state j

$$S^{(n)}(t_n,\ldots,t_1)=\sum_{jl}G_{jl}^{(n)}(t_n,\ldots,t_1)[\rho_\nu]_l(0). \tag{24}$$

For a Markovian modulation of bath jumps, the stochastic Liouville equation [Eq. (13)] may be readily used to calculate Green functions and multipoint quantities. For nonmarkovian processes, such as CTRW, the Green function may not be factorized into two point quantities. For a general $\psi(t)$ we must use recurrence relations to express higher order correlations functions in terms of lower ones [18]. We define a matrix $\hat{R}^{(k)}(t_k,\ldots,t_1)$, whose jl element represents the density of contributions to $S^{(k)}(t_k,\ldots,t_1)$ from paths which started in state l at τ_0 and a jump had occurred exactly at

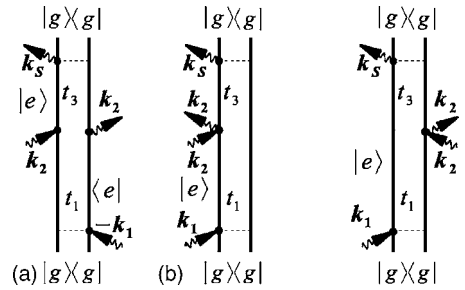

FIG. 3. (a) Double sided Feynman diagram for two pulse photon echo technique—response in $\mathbf{k}_S=2\mathbf{k}_2-\mathbf{k}_1$ direction. (b) Two double sided Feynman diagrams for the response in the $\mathbf{k}_S=\mathbf{k}_1+\mathbf{k}_2-\mathbf{k}_2$ direction.

time $\tau_k(=\tau_0+\Sigma_{i=1}^{k}t_i)$ to state j. $\hat{R}^{(k)}$ is $\hat{G}^{(k)}$ restricted to paths with a jump at τ_k. It may be factorized into a product of factors representing all jumps up to the last one preceding τ_k (say at τ_k') and the contribution $\hat{\Psi}(\tau_k-\tau_k')\exp[\int_{\tau_k'}^{\tau_k}\hat{L}(\tau')d\tau']$ from the Liouville space evolution from that moment in a fixed state of the bath. The jump preceding τ_k could occur either in the same time interval [the second term in Eq. (25)] or during any of the previous intervals. The latter contributions are described by another matrix $\hat{\Xi}^{(k)}(t_k,\ldots,t_1)$ whose jl element represents the density of contributions to $S^{(k)}\times(t_k,\ldots,t_1)$ from paths which started in state l at τ_0 and where the *first* jump after $\tau_{k-1}(=\tau_0+\Sigma_{i=1}^{k-1}t_i)$ had occured exactly at time τ_k to state j. This leads to the following equation for $\hat{R}^{(k)}$

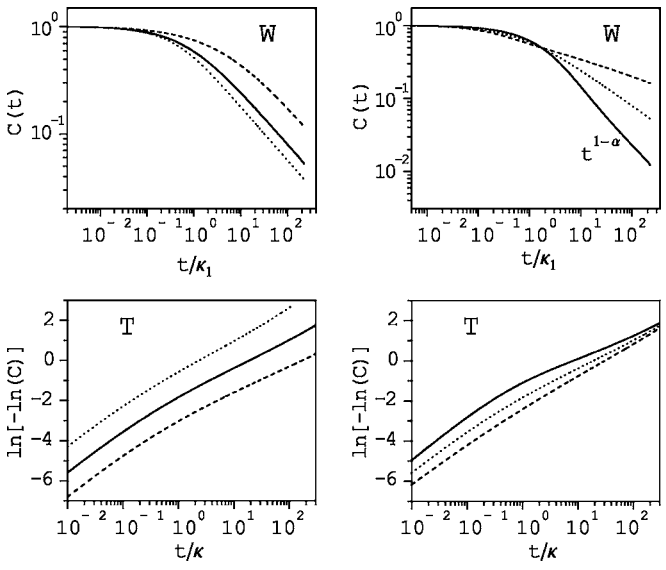

FIG. 4. Frequency correlation function $C(t)\equiv\langle\delta\omega_{eg}(t)\delta\omega_{eg}(0)\rangle/\omega_0^2$ [Eq. (31)]. Top row: W model with (top left panel) changing $\kappa_\alpha/\kappa_1=1$ (dotted line), 2 (solid line), 10 (dashed line) for ($\alpha=1.5$) or (top right panel) varying $\alpha=1.3$ (dashed line), 1.5 (solid line), 1.7 (dotted line) (for $\kappa_\alpha/\kappa_1=2$). Bottom row: T model with (bottom left panel) changing $\kappa\lambda=0.1$ (dotted line), 0.01(solid line), 0.001 (dashed line) for $\alpha=0.5$ and with (bottom right panel) changing $\alpha=0.3$ (dashed line), 0.5 (dotted line), 0.7 (solid line) for $\kappa\lambda=0.01$.

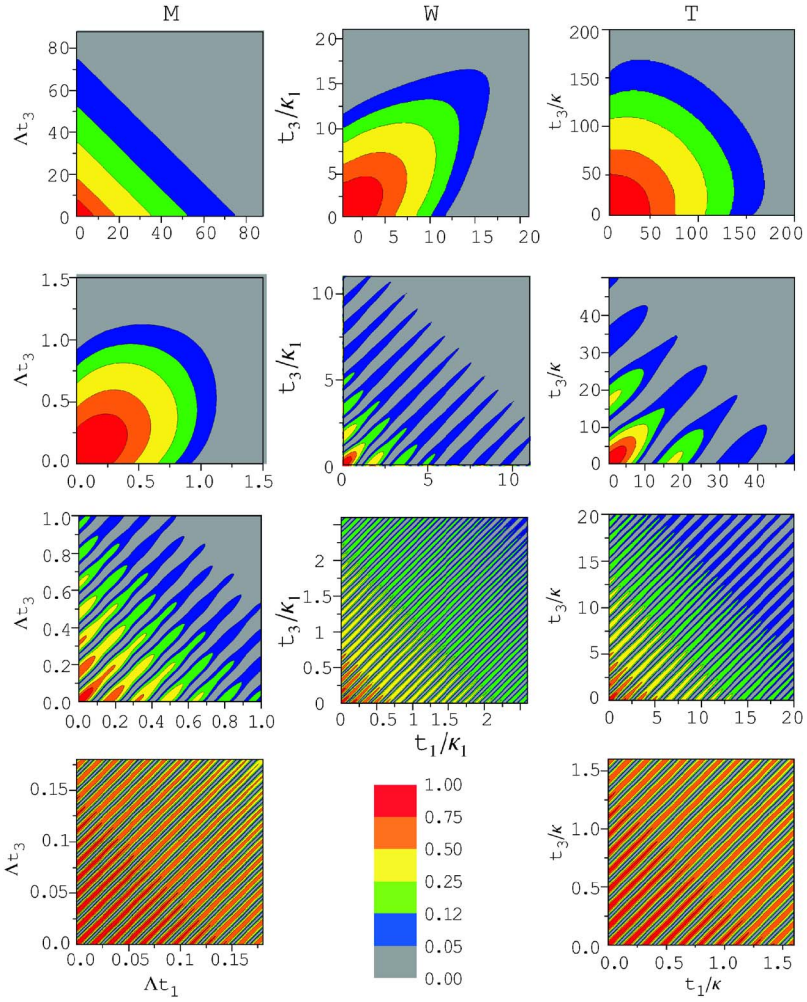

FIG. 5. (Color online) The photon echo signal [Eq. (C1)] for model M (left panels), W (central panels), and T (right panels). The parameters interpolate from the fast (upper panels) to slow fluctuation limit (bottom panels). Parameters as used for the absorption line shapes in Fig. 1.

$$\hat{R}^{(k)}(t_k,\ldots,t_1) = \hat{\Xi}^{(k)}(t_k,\ldots,t_1) + \int_0^{t_k} dt_k' \hat{\Psi}(t_k - t_k') \times \exp[\hat{L}^{(k)}(t_k - t_k')]\hat{R}^{(k)}(t_k', t_{k-1},\ldots,t_1). \tag{25}$$

To calculate $\hat{\Xi}^{(k)}$ we need to sum over all possible realizations of the jump before the last to occur in some previous time interval $t_{j<k}$.

$$\hat{\Xi}^{(k)}(t_k,\ldots,t_1) = \hat{\Psi}'\left(\sum_{i=1}^{k} t_i\right)\exp\left[\sum_{q=1}^{k}\hat{L}^{(q)}t_q\right] + \sum_{j=1}^{k-1}\int_0^{t_j}\hat{\Psi}\left(\sum_{i=j}^{k} t_i - t_j'\right) \times \exp\left[-\hat{L}^{(j)}t_j' + \sum_{q=j}^{k}\hat{L}^{(q)}t_q\right]\hat{R}^{(j)}(t_j', t_{j-1},\ldots,t_1)dt_j'. \tag{26}$$

The first term represents paths with only a single jump (at τ_k).

Equations (25) and (26) form a closed system for $\hat{\Xi}^{(k)}$ and $\hat{R}^{(k)}$, given $\hat{R}^{(j)}$ for $j<k$. These can be solved recursively starting with $R^{(1)}$ [Eq. (15)]. The Green function is finally obtained by

$$\hat{G}^{(n)}(t_n,\ldots,t_1) = \hat{\Phi}'\left(\sum_{i=1}^{n} t_i\right)\exp\left[\sum_{q=1}^{n}\hat{L}^{(q)}t_q\right] + \sum_{k=1}^{n}\int_0^{t_k}\hat{\Phi}\left(\sum_{i=k}^{n} t_i - t_k'\right) \times \exp\left[\hat{L}^{(k)}(t_k - t_k') + \sum_{q=k+1}^{n}\hat{L}^{(q)}t_q\right] \times \hat{R}^{(k)}(t_k', t_{k-1},\ldots,t_1)dt_k'. \tag{27}$$

The solution to Eqs. (25)–(27) is given in Laplace space by the recurrence relations developed in Appendix B, and $S_\nu^{(n)}$ is finally calculated using Eq. (24). These results recover the two-point correlation functions [Eqs. (15) and (16)].

IV. THE THIRD-ORDER RESPONSE

We have applied our recursion relations to calculate the third order polarization:

$$P^{(3)}(t) = \int_0^\infty dt_3 \int_0^\infty dt_2 \int_0^\infty dt_1 S^{(3)}(t_3,t_2,t_1) \times E(t-t_3)E(t-t_3-t_2)E(t-t_3-t_2-t_1).$$

$S^{(3)}$ is obtained by setting $\delta\omega^{(2)}=0$ and $\delta\omega^{(1)}=\pm\delta\omega^{(3)}$ into

Eq. (22), the various signs correspond to different Liouville space pathways ν.

We first consider the limit when the time intervals t_1 and t_3 are short compared to the random walk timescale κ. The Liouville space contributions for these intervals then factorize as $\exp(\pm i\omega_0-\Gamma)t_j$, $j=1,3$ and the response only depends on the two point joint probability density function P for CTRW

$$S^{(3)}(t_3,t_2,t_1)=\sum_{x_1=a,b}\sum_{x_2=a,b}P(x_2x_1,t_2)e^{i\delta\omega_{x_1}t_1}e^{\pm i\delta\omega_{x_2}t_3}. \quad (28)$$

This response function which is related to hole-burning spectroscopy [15] can be expressed in terms of ordinary two point frequency correlation function $C(t)\equiv\langle\delta\omega_{eg}(t)\delta\omega_{eg}(0)\rangle/\omega_0^2=P(aa)+P(bb)-P(ba)-P(ab)$ as

$$S^{(3)}(t_3,t_2,t_1)=[\cos(\omega_0t_1)\cos(\omega_0t_3) \mp C(t_2)\sin(\omega_0t_1)\sin(\omega_0t_3)]/2. \quad (29)$$

The two-point joint probability distribution function for our TSJ models is

$$\tilde{P}(aa,s)=\tilde{P}(bb,s)=\frac{1}{2s}-\frac{\tilde{\psi}'(s)}{2s(1+\tilde{\psi}(s))}$$

and

$$\tilde{P}(ab;s)=\tilde{P}(ba;s)=\frac{\tilde{\psi}'(s)}{2s(1+\tilde{\psi}(s))}. \quad (30)$$

By combining Eq. (10) with Eq. (30) the correlation function is given in the Laplace space by

$$\tilde{C}(s)=\frac{1}{s}-\frac{2(1-\tilde{\psi}(s))}{\bar{t}s^2(1+\tilde{\psi}(s))}. \quad (31)$$

The Markovian model gives a simple exponential decay $C_M(t)=e^{-2\Lambda t}$. For the W model the correlation function is

$$\tilde{C}_W(s)=\frac{1}{s}\left[1-\frac{1}{1+(\kappa_\alpha s)^{\alpha-1}+\kappa_1 s/2}\right]$$

with the long time power laws $C_W(t)\approx(\kappa_\alpha/t)^{\alpha-1}$ as shown at Fig. 4, top row. κ_α/κ_1 varied in the left panel, determines the time scale when the long-time behavior is reached. In the right panel we varied α parameter which determines the asymptotic slope $C_W(t)\propto 1/t^{\alpha-1}$. This long time form can be attributed to dominant contributions of the nonfluctuating particles $\phi'(t)$.

The correlation function for the T model is displayed in the lower panel

$$\tilde{C}_T(s)=\frac{1}{s}\left[1+\frac{\lambda[1+(\kappa\lambda)^\alpha][1-(1+s/\lambda)^\alpha]}{s\alpha(1+(\kappa_\alpha\lambda)^\alpha[1+(1+s/\lambda)^\alpha]/2)}\right].$$

The complete third-order response function is calculated in Appendix D. Assuming $t_2=0$, the response function which depends on two-intervals t_1, t_3 can be expressed in the form

$$\begin{aligned}\hat{\tilde{G}}^{(3)}(s_3,t_2=0,s_1)=&\hat{\tilde{\Phi}}(s_3-\hat{L}^{(3)})[1-\hat{\tilde{\Psi}}(s_3-\hat{L}^{(3)})]^{-1}(\hat{\tilde{\Psi}}'(s_1-\hat{L}^{(1)})-\hat{\tilde{\Psi}}'(s_3-\hat{L}^{(3)}))\frac{1}{s_3-\hat{L}^{(3)}-s_1+\hat{L}^{(1)}}+\hat{\tilde{\Phi}}(s_3-\hat{L}^{(3)})\\&\times[1-\hat{\tilde{\Psi}}(s_3-\hat{L}^{(3)})]^{-1}(\hat{\tilde{\Psi}}(s_3-\hat{L}^{(3)})-\hat{\tilde{\Psi}}(s_1-\hat{L}^{(1)}))\frac{1}{(s_1-\hat{L}^{(1)}-s_3+\hat{L}^{(3)})}[1-\hat{\tilde{\Psi}}(s_1-\hat{L}^{(1)})]^{-1}\hat{\tilde{\Psi}}'(s_1-\hat{L}^{(1)})\\&+(\hat{\tilde{\Phi}}(s_3-\hat{L}^{(3)})-\hat{\tilde{\Phi}}(s_1-\hat{L}^{(1)}))\frac{1}{(s_1-\hat{L}^{(1)}-s_3+\hat{L}^{(3)})}[1-\hat{\tilde{\Psi}}(s_1-\hat{L}^{(1)})]^{-1}\hat{\tilde{\Psi}}'(s_1-\hat{L}^{(1)})\\&+(\hat{\tilde{\Phi}}'(s_3-\hat{L}^{(3)})-\hat{\tilde{\Phi}}'(s_1-\hat{L}^{(1)}))\frac{1}{s_1-\hat{L}^{(1)}-s_3+\hat{L}^{(3)}},\end{aligned} \quad (32)$$

where s_1, s_3 are the Laplace conjugates to t_1 and t_3, respectively. This correlation function represents the two-pulse experiment shown in the double sided Feynman diagram (Fig. 3.)

We consider the pathway Fig. 3(a) by applying Eq. (32) with $\hat{L}^{(1)}=-\hat{L}^{(3)}$. The first pulse (with wave vector $\mathbf{k}_1$) creates a coherence and the second pulse (wave vector $\mathbf{k}_2$) reverses it. The photon echo signal is detected after time t_3+t_1 in the direction $\mathbf{k}_S=2\mathbf{k}_1-\mathbf{k}_2$. Assuming a large static inhomogenous broadening the signal rapidly vanishes except for $t_1=t_3$.

For the other Feynman diagrams [Fig. 3(b)] represent the signal in the $\mathbf{k}_s=\mathbf{k}_1$ direction and we set $\hat{L}^{(1)}=\hat{L}^{(3)}$ in Eq. (32). The interaction at t_1 does not change the state of the system. The response is described by the two point function and carries no additional information compared to the linear response.

The response function for the pathway [Fig. 3(a)] which may be obtained by substituting Eqs. (A3)–(A5) in Eq. (32) is given by Eq. (C1). We first discuss two limiting cases for the Markovian model. For fast fluctuations $\Lambda>\omega_0$ we get by inverting Eq. (C2)

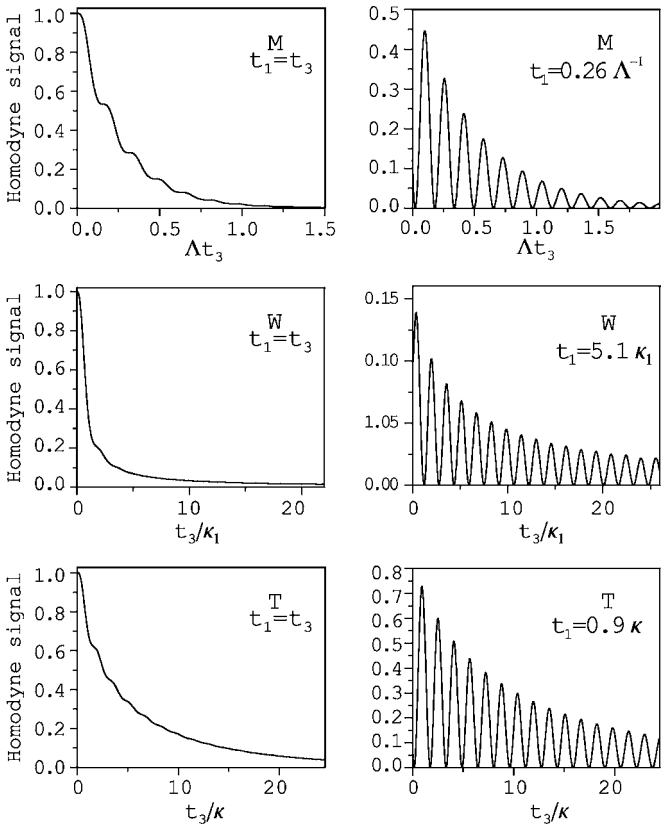

FIG. 6. The photon echo signal [Eq. (C1)] is plotted at the diagonal $t_1=t_3$ (left panels) and fixed t_1 sections (right panels) for M (upper panel) $\omega_0/\Lambda=20$, W (central panel) $\alpha=1.5$, $\kappa_1/\kappa_\alpha=0.5$, $\omega_0\kappa_1=2$, and T (lower panel) ($\kappa\lambda=0.01$, $\alpha=0.5$, $\omega_0\kappa=2$) models.

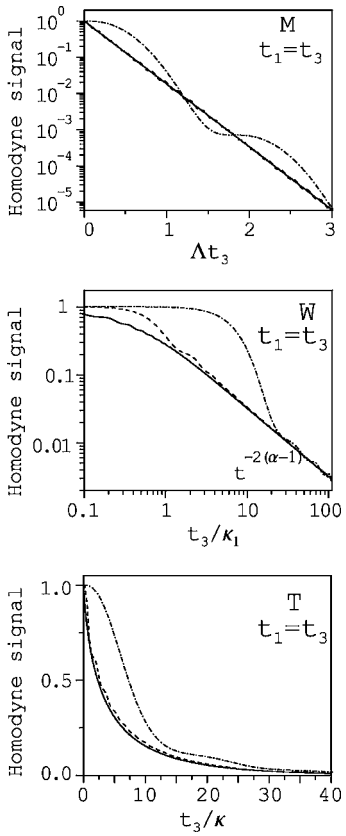

FIG. 7. The diagonal $t_1=t_3$ section of the photon echo signal [Eq. (C1)]. Transition from fast (dash-dotted lines, ω_0/Λ, $\omega\kappa\to 0$) to slow fluctuations (solid lines, ω_0/Λ, $\omega_0\kappa\to\infty$) is shown for the M (upper panel), T (central panel), and W (lower panel) models for parameters used. M: $\omega_0/\Lambda=2$ (dash-dotted line), 20 (solid line), 200 (dashed line). T: $\alpha=0.5$, $\kappa\lambda=0.01$, $\kappa\omega_0=0.2$ (dash-dotted line), 2 (dashed line), 20 (solid line). W: $\alpha=1.5$, $\kappa_1/\kappa_\alpha=1.5$, $\kappa_1\omega_0=0.2$ (dash-dotted line), 2 (dashed line), 20 (solid line).

$$S^{(3)}(t_3,0,t_1)=e^{-\Lambda(t_3+t_1)}\left(-\frac{\omega_0^2}{\eta^2}\cosh[\eta(t_3-t_1)]+\frac{\Lambda^2}{\eta^2}\cosh[\eta(t_3+t_1)]+\frac{\Lambda}{\eta}\sinh[\eta(t_3+t_1)]\right), \tag{33}$$

where $\eta=\sqrt{\Lambda^2-\omega_0^2}$.

More interesting is the opposite case $\omega_0>\Lambda$ where

$$S^{(3)}(t_3,0,t_1)=e^{-\Lambda(t_3+t_1)}\left(\frac{\omega_0^2}{\xi^2}\cos[\xi(t_3-t_1)]-\frac{\Lambda^2}{\xi^2}\cos[\xi(t_3+t_1)]+\frac{\Lambda}{\xi}\sin[\xi(t_3+t_1)]\right), \tag{34}$$

and $\xi=\sqrt{\omega_0^2-\Lambda^2}$

The impulsive response to short pulses is given by

$$P^{(3)}(t_1+t_3)=\left(\frac{i}{\hbar}\right)^3 E_2E_2^*E_1S^{(3)}(t_3,0,t_1).$$

The signal is finally obtained by

$$M(t_3,t_1)\approx|P^{(3)}(t_1+t_3)|^2. \tag{35}$$

Figure 5 shows the photon echo signal [Eqs. (C1) and (35)] for models M (left column), W (middle column), and T (right column). The calculations interpolate between the fast (upper panels) to the slow (lower panels) fluctuation limits. Each panel in Fig. 5 has a corresponding panel in Fig. 1.

The photon echo peak at $t_1=t_3$ is known to dominate the response of systems with large disorder. In the static limit this arises from a constructive interference from two contributions with phase $\pm\omega_0(t_3-t_1)$ attributed to a particular state of bath. For the present TSJ model, interference exists not only for $t_1=t_3$ but whenever the phases differ by $2\pi k$ and the response shows oscillations along t_3 with period $2\pi/\omega_0$. Small oscillations best show at the diagonal ($t_1=t_3$) slice in Fig. 6. For M these correspond to the second and the third terms in Eq. (34). The differences show up in the decay of the envelope which is subexponential for W and T, compared to exponential for M.

The M signal (left panel of Fig. 5) is dominated by the first term of Eq. (34), showing $\cos^2(\omega_0(t_1-t_3))$ oscillations with exponential decay $e^{-2\Lambda(t_1+t_3)}$. The ratio ω_0/Λ is varied in Fig. 5. Decreasing this parameter shows a transition from

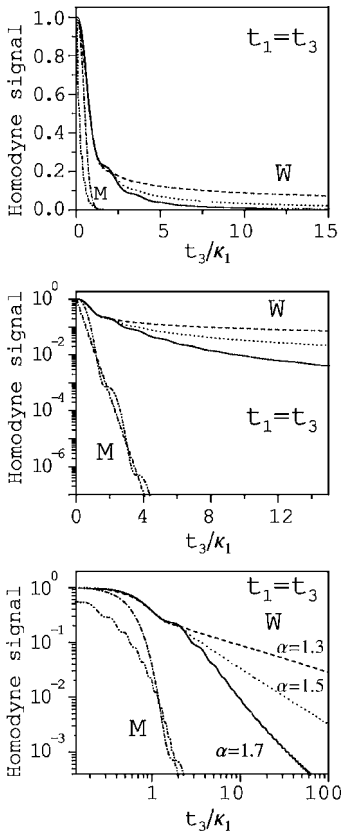

FIG. 8. The diagonal $t_1=t_3$ section of the photon echo signal. We compare the W and M models using linear plots (upper panel), linear-log plot (central panel, exponential function e^{-t} becomes straight lines) and log-log plots (lower panel, power laws become straight lines) for parameters. W: $\kappa_\alpha/\kappa_1=2$, $\omega_0\kappa_1=2$ and $\alpha=1.3$ (solid line), 1.5 (dotted line), 1.7 (dashed line); M: $\kappa_1=\Lambda^{-1}$, $\omega_0/\Lambda=\omega\kappa_1=2$ (dot-dashed line), and $\omega_0/\Lambda=20$ (dash-dot-dotted line).

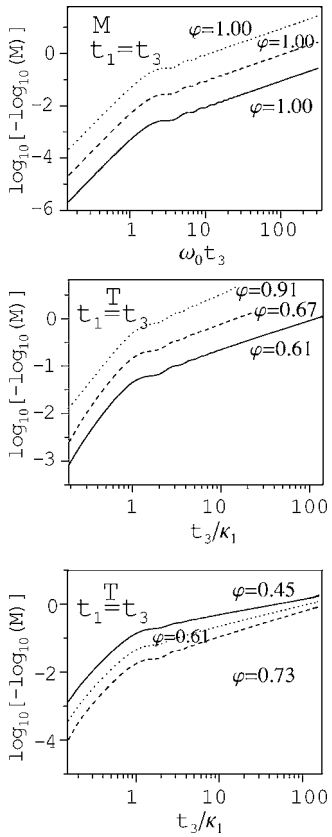

FIG. 9. The diagonal $t_1=t_3$ section for the photon echo signal. The $\log t$ vs $\log[-\log M(t,0,t)]$ plot shows the stretched exponential decays as straight lines. Relaxation is exponential for M (upper panel) in all cases $\omega_0/\Lambda=20$ (dotted line), 200 (dashed line), and 2000 (solid line). Model T is well fitted to stretched exponential e^{-t^φ} with complex dependence on both cutoff (central panel), $\kappa\lambda=0.001$ (solid line), $\kappa\lambda=0.01$ (dashed line), $\kappa\lambda=0.1$ (dotted line) for ($\alpha=0.5$, $\omega_0\kappa=2$), and α (lower panels), $\alpha=0.3$ (dashed), 0.5 (dotted line), 0.7 (solid line) (for $\kappa\lambda=0.001$, $\omega_0\kappa=2$).

oscillations (lower panel) to damped signal (upper panel), the oscillatory modulation at $t_1=t_3$ slope becomes important in accordance with the Λ/ξ factor in Eq. (34) and the oscillation period ($2\pi/\sqrt{\omega_0^2-\Lambda^2}$) becomes longer. The middle column shows the transition from fast fluctuations $\omega_0\kappa_1=0.2$ (upper panel) to slow fluctuations $\omega_0\kappa_1=20.0$ (lower panel) for the W model. The long tailed power law asymptotic decay of the signal is observed in both limits as there is no time scale where the fraction of nonfluctuating particle becomes exponentially small, in contrast to M (and T).

Figure 7 compares the effect of slow and fast fluctuations by varying ω_0 for $t_1=t_3$. In all cases as ω_0 is decreased the solution oscillates around the large ω_0 limit. The long time power laws are further shown in Fig. 8 for the W model with varying α together with the M model with the same $\kappa_1=\Lambda^{-1}$ and the same $\omega_0\kappa=2$ (dash-dotted line) or $\omega_0\kappa=20$ (dash-dot-dotted line). The linear-linear plot shows the rapid Markovian relaxation compared the W model, this is further shown by linear-log plot (middle panel, exponential function is linear) and log-log plot (lower panel, power law is linear).

Asymptotically the correlation function for CTRW with long-tailed WTDF reflects the the fraction of particles that did not move as described by a survival function for the first jumps $\phi'(t)$. This nomenclature is somewhat unfortunate, since $\phi'(t)$ represents the stationary state and not simply the first jump probability. The ensemble becomes stationary after some time, no matter how fast the initial jump is. Right after the jump the particle has a higher probability to jump again than a particle residing at one position for a long time as $\psi_W(t)/\phi_W(t)\propto\alpha/t$ (for $t\to\infty$). The contribution of the fluctuating particles thus vanishes asymptotically more rapidly. The W model has $\phi'(t)\propto 1/t^{\alpha-1}$ with correlation function $C_W(t)\propto 1/t^{\alpha-1}$, the peaks in linear absorption $I(\omega+\omega_0+\omega_{eg})\propto\omega^{\alpha-2}$ and the photon echo signal $M_W(t_3,t_1)\propto 1/(t_1+t_3)^{2(\alpha-1)}$.

To demonstrate the capability of nonlinear spectroscopy to distinguish between various models of anomalous spectral diffusion with the same peak in linear line shape we assume the same peak in linear absorption we consider the Brownian oscillator model (Gaussian bath) [15] with peak $I(\omega)\propto\omega^{\alpha-2}$ corresponding to $S^{(1)}(t_1)\propto 1/t_1^{\alpha-1}$. The Brownian oscillator model is fully described by the line broadening function $g(t)$, connected to response function $S_G^{(1)}(t_1)=\exp[-g(t_1)]$. The third order response function for the diagram Fig. 3(a) is recast using cumulants [15]

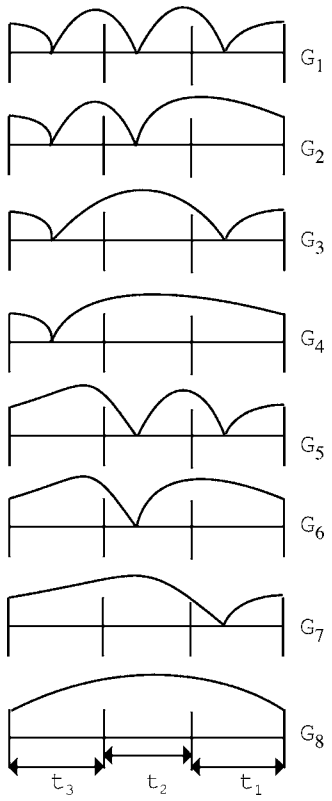

FIG. 10. Diagram for the $\hat{G}_1$-$\hat{G}_8$ contributions to the Green function Eq. (D3) for the third order response. Contributions represent paths with (line meets the axis) or without (line does not meet the axis) some jump in the particular time interval.

$$S_G^{(3)}(t_3,0,t_1) = \exp[-g(t_1) - g^*(t_1) - 2g^*(t_3) + g^*(t_3+t_1)] = |S^{(1)}(t_1)|^2[S^{(1)*}(t_3)]^2[S^{(1)*}(t_1+t_3)]^{-1}. \quad (36)$$

The photon echo signal [Eq. (35)] at $t_1=t_3$ for the Gaussian model decays as $M_G(t,t) \propto 1/t^{6(\alpha-1)}$ whereas for W model $M_W(t,t) \propto 1/t^{2(\alpha-1)}$.

The photon echo for the T model (Fig. 5, right column) is qualitatively similar to M: it has ω_0 oscillations, slight oscillatory modulation at $t_1=t_3$ slices and the slow and fast limit. The T model has three timescales $\omega_0, \kappa, \lambda$. The role of κ, λ was discussed in [18].

The right column displays various values of $\omega_0\lambda$ with fixed $\kappa\lambda=0.01$. It again shows the transition between damped $\omega_0/\lambda=0$ and oscillatory $\omega_0/\lambda=0$ limits. Besides the effects seen for M we observe a subexponential decay. In an earlier study [18] we provided fit of the frequency correlation function to a stretched exponential, $f(t) \sim e^{-t^{\varphi}}$ which is depicted as linear in $\log(-\log[f(t)])$ vs $\log(t)$ with slopes determined by φ.

The diagonal decay plots $\log\{-\log[M(t_3=t,t_1=t)]\}$ vs $\log(t)$ are shown in Fig. 9 for M and T. After the initial period $\omega_0 t < \pi$ we observe the straight lines slightly modulated by oscillations. The slopes calculated over this period show exponential decay $\varphi=1.0$ for the M (upper panel) and the subexponential values $\varphi<1$ for T (middle and lower panels). With increasing $\kappa\lambda$ the exponential relaxation is approached with complex dependence of φ on $\kappa\lambda$ (middle) and α (lower panel) similar to the frequency correlation function [18].

In summary, the photon echo signal with anomalous relaxation corresponds to a Markovian process except that the envelope decays similarly to the frequency correlation function [Eq. (31)]. Asymptotically this is given by the survival function for the first jump.

Secondary peaks or other sections (e.g., t_1 fixed, varying t_3 in left panel of Fig. 6) also show long-time subexponential decay. We expect the decay at $t_1=t_3$ to be the clearest sign of subexponential relaxation, because constructive interference is present for more disordered spectra, while the secondary peaks will be suppressed [15]. This is motivated by the asymptotic form for the W model

$$S^{(3)}(t_3,t_2,t_1) \propto \int d\omega C(t_1+t_2+t_3)\exp i\omega(t_3-t_1)\tilde{\Theta}(\omega) = C(t_1+t_2+t_3)\Theta(t_3-t_1),$$

where $\tilde{\Theta}(\omega)$ is the equilibrium density of particles with gap frequency ω and $\Theta(t)$ is its Fourier transform. The $f(t_3+t_1)g(t_3-t_1)$ functional form is compatible with our other results as the secondary peaks $\omega(t_3-t_1)=k\pi$ decay quite similarly to the diagonal peak for W.

V. DISCUSSION

We have simulated the nonlinear response function for a two-level system undergoing stochastic frequency fluctations. The stochastic Liouville equation approach is generalized for non-Markovian fluctuations. The continuous time random walk was used to model memory effects resulting from arbitrary waiting time distributions between successive jumps.

Applications were made to the photon echo signal for a TSJ model with anomalous bath kinetics and power law WTDF's. We found power law (or stretched exponential) long time decay, rather then exponential of the Markovian case, similar to the ordinary frequency correlation function of the frequency. For random walks with broad distributions of waiting times some particles remain trapped at their initial position. These particles may dominate the long time behavior and result in the anomalous kinetics. Similar trends have been seen for anomalous diffusion in a potential [10,18]. The present formalism may also be applied to photon statistics which for weak fields may be expressed in tems of four-point correlation functions [53,54].

Even though we only studied stationary ensembles, our recursive algorithm can be readily used to nonstationary random walks by a proper choice of the WTDF for the first jump. However, nonstationarity breaks down the time-translation invariance of correlation functions and the substitution $\psi'(t)=\psi(t)$ in Eqs. (15) and (16) does not give the absorption line shape as Eq. (2) is no longer valid [45]. For the same reasons the ensemble-averaged and time-averaged function are not identical for nonergodic CTRW so that $C(t)$ should not be applied in single molecule spectroscopy [42,55].

The results of Sec. III and Appendixes B and D may be extended for multistate bath or for continuous bath variable by constructing proper $\hat{L}$, $\hat{\Psi}$, and $\hat{\Phi}$ matrices. An interesting application will be to spectral diffusion in a harmonic potential [11,18].

ACKNOWLEDGMENTS

The support of Chemical Sciences, Geosciences and Biosciences Division, Office of Basic Energy Sciences, Office of Science, U.S. Department of Energy is gratefully acknowledged.

APPENDIX A: THE TWO-STATE-JUMP CTRW MODEL FOR LINE SHAPES

We introduce the Laplace space quantities

$$\hat{\tilde{R}}(s) \equiv \int_0^\infty e^{-st}\hat{R}(t)dt, \quad \hat{\tilde{\Psi}}(s-\hat{L}) \equiv \int_0^\infty e^{-st}\hat{\Psi}(t)\exp[\hat{L}t]dt,$$

$$\hat{\tilde{G}}(s) \equiv \int_0^\infty \hat{G}(t)e^{-st}dt, \quad \hat{\tilde{\Phi}}(s-\hat{L}) \equiv \int_0^\infty e^{-st}\hat{\Phi}(t)\exp[\hat{L}t]dt.$$

Equation (15) is then solved by

$$\hat{\tilde{R}}(s) = [1-\hat{\tilde{\Psi}}(s-\hat{L})]^{-1}\hat{\tilde{\Psi}}'(s-\hat{L}) \tag{A1}$$

and Eq. (16) reads

$$\hat{\tilde{G}}(s) = \hat{\tilde{\Phi}}'(s-\hat{L}) + \hat{\tilde{\Phi}}(s-\hat{L})\hat{\tilde{R}}(s). \tag{A2}$$

With Eqs. (8) and (9) we have

$$\hat{\tilde{\Psi}}(s-\hat{L}) = \begin{pmatrix} 0 & \tilde{\psi}(s-i\omega_0) \\ \tilde{\psi}(s+i\omega_0) & 0 \end{pmatrix}, \tag{A3}$$

$$\hat{\tilde{\Phi}}(s-\hat{L}) = \begin{pmatrix} \tilde{\phi}(s+i\omega_0) & 0 \\ 0 & \tilde{\phi}(s-i\omega_0) \end{pmatrix}. \tag{A4}$$

For the TSJ model the propagator is straightforwardly calculated as

$$[1-\hat{\tilde{\Psi}}(s-\hat{L})]^{-1} = \frac{1}{1-\tilde{\psi}(s+i\omega_0)\tilde{\psi}(s-i\omega_0)} \times \begin{pmatrix} 1 & \tilde{\psi}(s-i\omega_0) \\ \tilde{\psi}(s+i\omega_0) & 1 \end{pmatrix} \tag{A5}$$

and by combining Eqs. (A1)–(A5) the Green function is solved

$$\tilde{G}_{aa}(s) = \tilde{\phi}'(s+i\omega_0) + \frac{\tilde{\phi}(s+i\omega_0)\tilde{\psi}(s-i\omega_0)\tilde{\psi}'(s+i\omega_0)}{1-\tilde{\psi}(s-i\omega_0)\tilde{\psi}(s+i\omega_0)},$$

$$\tilde{G}_{ab}(s) = \frac{\tilde{\phi}(s+i\omega_0)\tilde{\psi}'(s-i\omega_0)}{1-\tilde{\psi}(s-i\omega_0)\tilde{\psi}(s+i\omega_0)},$$

$$\tilde{G}_{ba}(s) = \frac{\tilde{\phi}(s-i\omega_0)\tilde{\psi}'(s+i\omega_0)}{1-\tilde{\psi}(s-i\omega_0)\tilde{\psi}(s+i\omega_0)},$$

$$\tilde{G}_{bb}(s) = \tilde{\phi}'(s-i\omega_0) + \frac{\tilde{\phi}(s-i\omega_0)\tilde{\psi}(s+i\omega_0)\tilde{\psi}'(s-i\omega_0)}{1-\tilde{\psi}(s-i\omega_0)\tilde{\psi}(s+i\omega_0)}. \tag{A6}$$

Setting Eqs. (10) and (A6) to Eq. (12) gives Eq. (17).

APPENDIX: B RECURRENCE RELATIONS FOR MULTIPOINT CORRELATION FUNCTIONS

To derive the 4-point nonlinear response function, we start by solving Eqs. (26) and (25) by introducing Laplace space conjugates to $t_1, \ldots, t_k$

$$\hat{\tilde{\tilde{R}}}^{(k)}(s_k, \ldots, s_1) = \int_0^\infty \cdots \int_0^\infty e^{-\Sigma_{j=1}^k s_j t_j}\hat{R}^{(k)}(t_k, \ldots, t_1)dt_1 \ldots dt_k$$

and similary for the matrices $\hat{G}, \hat{\Xi}$.

The solution of Eq. (25) is

$$\hat{\tilde{\tilde{R}}}^{(k)}(s_k, \ldots, s_1) = [1-\hat{\tilde{\Psi}}(s_k-\hat{L}^{(k)})]^{-1}\hat{\tilde{\tilde{\Xi}}}^{(k)}(s_k, \ldots, s_1) \tag{B1}$$

and Eq. (26) gives

$$\begin{aligned}\hat{\tilde{\tilde{\Xi}}}^{(k)}(s_k, \ldots, s_1) &= \int_{-i\infty}^{i\infty} \frac{ds_k^*}{2\pi i}\hat{\tilde{\Psi}}'(s_k^*)\prod_{q=1}^{k}\frac{1}{s_q-\hat{L}^{(q)}-s_k^*} \\ &+ \sum_{j=1}^{k-1}\int_{-i\infty}^{i\infty}\int_{-i\infty}^{i\infty}\frac{ds_j'}{2\pi i}\frac{ds_k^*}{2\pi i}\hat{\tilde{\Psi}}(s_k^*)\left[\frac{1}{s_j-s_j'}-\frac{1}{s_j-\hat{L}^{(j)}-s_k^*}\right] \\ &\times\frac{1}{s_j'-s_k^*-\hat{L}^{(j)}}\prod_{q=j+1}^{k}\frac{1}{s_q-\hat{L}^{(q)}-s_k^*}\hat{\tilde{\tilde{R}}}^{(j)}(s_j', s_{j-1}, \ldots s_1).\end{aligned} \tag{B2}$$

The Green function Eq. (27) is also obtained in Laplace space

$$\begin{aligned}\hat{\tilde{\tilde{G}}}^{(n)}(s_n, \ldots, s_1) &= \int_{-i\infty}^{i\infty}\frac{ds_n^*}{2\pi i}\hat{\tilde{\Phi}}'(s_n^*)\prod_{q=1}^{n}\frac{1}{s_q-\hat{L}^{(q)}-s_n^*} + \hat{\tilde{\Phi}}(s_n-\hat{L}^{(n)})\hat{\tilde{\tilde{R}}}^{(n)} \\ &\times(s_n, \ldots, s_1) + \sum_{k=1}^{n-1}\int_{-i\infty}^{i\infty}\frac{ds_k'}{2\pi i}\int_{-i\infty}^{i\infty}\frac{ds_n^*}{2\pi i}\hat{\tilde{\Phi}}(s_n^*)\left[\frac{1}{s_k-s_k'}\right. \\ &\left.-\frac{1}{s_k-\hat{L}^{(k)}-s_n^*}\right]\times\frac{1}{s_k'-s_n^*-\hat{L}^{(k)}}\prod_{q=k+1}^{n}\frac{1}{s_q-\hat{L}^{(q)}-s_n^*} \\ &\times\hat{\tilde{\tilde{R}}}^{(k)}(s_k', s_{k-1}\ldots;s_1).\end{aligned} \tag{B3}$$

The residue theorem can be used to integrate Eqs. (B2) and (B3). Finally the nth interval correlation function is

a sum of 2^n contribution each characterized by whether some jumps occurred or not in particular interval. Figure 10 shows diagrams for particular case of the third order response function which are interpreted as follows: The jumps occurred in intervals where the line touches the time axis. The particular contribution is a matrix product of the following factors.

If there is some jump in the kth interval one should account $[1-\hat{\tilde{\Psi}}(s_k-\hat{L}^{(k)})]^{-1}$ for propagation through kth interval.

For the jump from kth to $(k+1)$th interval one should account for $(\hat{\tilde{\Psi}}(s_{k+1}-\hat{L}^{(k+1)})-\hat{\tilde{\Psi}}(s_k-\hat{L}^{(k)}))\ [s_k-\hat{L}^{(k)}-s_{k+1}-\hat{L}^{(k+1)}]^{-1}$.

For the jump from kth to $(k+2)$th interval

$$\hat{\tilde{\Psi}}(s_{k+2}-\hat{L}^{(k+2)}) \times\frac{1}{s_{k+1}-\hat{L}^{(k+1)}-s_{k+2}+\hat{L}^{(k+2)}}\frac{1}{s_k-\hat{L}^{(k)}-s_{k+2}+\hat{L}^{(k+2)}} + \hat{\tilde{\Psi}}(s_{k+1}-\hat{L}^{(k+1)}) \times\frac{1}{s_{k+2}-\hat{L}^{(k+2)}-s_{k+1}+\hat{L}^{(k+1)}}\frac{1}{s_k-\hat{L}^{(k)}-s_{k+1}+\hat{L}^{(k+1)}} + \hat{\tilde{\Psi}}(s_k-\hat{L}^{(k)}) \times\frac{1}{s_{k+2}-\hat{L}^{(k+2)}-s_k+\hat{L}^{(k)}}\frac{1}{s_{k+1}-\hat{L}^{(k+1)}-s_k+\hat{L}^{(k)}}.$$

For the third order response jumps over more periods do not occur. For higher order a specific term is given by integrations of the second term in (B3) for any number of intervals in between successive jumps.

The factors $\hat{\tilde{\Psi}}'(s_1-L^{(1)})$, $\hat{\tilde{\Phi}}(s_n-L^{(n)})$ for the first jump or surviving from the last jump respectively if the first jump is in the first interval (survival is from the last interval). In case the first jump only comes in later intervals we have the same factor as above with replacing $\Psi\rightarrow\Psi'$, $\Phi\rightarrow\Phi'$.

APPENDIX C: THIRD-ORDER RESPONSE FOR TWO STATE JUMP MODEL

By substituting Eqs. (A3)–(A5) in Eq. (32) we get the response function for the pathway given in Fig. 3(a)

$$\begin{aligned}
2\tilde{S}^{(3)}(s_3,t_2=0,s_1) &= \frac{[\tilde{\phi}(s_3-i\omega_0)+\tilde{\phi}(s_3+i\omega_0)\tilde{\psi}(s_3-i\omega_0)]}{[1-\tilde{\psi}(s_3+i\omega_0)\tilde{\psi}(s_3-i\omega_0)][(1-\tilde{\psi}(s_1-i\omega)\tilde{\psi}(s_1+i\omega_0)\ ]}\\
&\times\frac{[\tilde{\psi}(s_3+i\omega_0)-\tilde{\psi}(s_1-i\omega_0)][\tilde{\psi}(s_1+i\omega_0)\tilde{\psi}'(s_1-i\omega_0)+\tilde{\psi}'(s_1+i\omega_0)]}{s_1-i\omega_0-s_3-i\omega_0}\\
&+\frac{[\tilde{\phi}(s_3+i\omega_0)+\tilde{\phi}(s_3-i\omega_0)\tilde{\psi}(s_3+i\omega_0)]}{[1-\tilde{\psi}(s_3+i\omega_0)\tilde{\psi}(s_3-i\omega_0)][1-\tilde{\psi}(s_1-i\omega_0)\psi(s_1+i\omega_0)]}\\
&\times\frac{[\tilde{\psi}(s_3-i\omega_0)-\tilde{\psi}(s_1+i\omega_0)][\tilde{\psi}(s_1-i\omega_0)\tilde{\psi}'(s_1+i\omega_0)+\tilde{\psi}'(s_1-i\omega_0)]}{s_1+i\omega_0-s_3+i\omega_0}\\
&+\frac{[\tilde{\phi}(s_3+i\omega_0)\tilde{\psi}(s_3-i\omega_0)+\tilde{\phi}(s_3-i\omega_0)][\tilde{\psi}'(s_3+i\omega_0)-\tilde{\psi}'(s_1-i\omega_0)]}{[1-\tilde{\psi}(s_3+i\omega_0)\tilde{\psi}(s_3-i\omega_0)][s_1-i\omega_0-s_3-i\omega_0]}\\
&+\frac{[\tilde{\phi}(s_3-i\omega_0)\tilde{\psi}(s_3+i\omega_0)+\tilde{\phi}(s_3+i\omega_0)][\tilde{\psi}'(s_3-i\omega_0)-\tilde{\psi}'(s_1+i\omega_0)]}{[1-\tilde{\psi}(s_3+i\omega_0)\tilde{\psi}(s_3-i\omega_0)][s_1+i\omega_0-s_3+i\omega_0]}\\
&+\frac{[\tilde{\phi}(s_3+i\omega_0)-\tilde{\phi}(s_1-i\omega_0)][\tilde{\psi}(s_1+i\omega_0)\tilde{\psi}'(s_1-i\omega_0)+\tilde{\psi}'(s_1+i\omega_0)]}{[s_1-i\omega_0-s_3-i\omega_0][1-\tilde{\psi}(s_1-i\omega_0)\tilde{\psi}(s_1+i\omega_0)]}\\
&+\frac{[\tilde{\phi}(s_3-i\omega_0)-\tilde{\phi}(s_1+i\omega_0)][\tilde{\psi}(s_1-i\omega_0)\tilde{\psi}'(s_1+i\omega_0)+\tilde{\psi}'(s_1-i\omega_0)]}{[s_1+i\omega_0-s_3+i\omega_0][1-\tilde{\psi}(s_1-i\omega_0)\tilde{\psi}(s_1+i\omega_0)]}+\frac{\tilde{\phi}'(s_3+i\omega_0)-\tilde{\phi}'(s_1-i\omega_0)}{s_1-i\omega_0-s_3-i\omega_0}\\
&+\frac{\tilde{\phi}'(s_3-i\omega_0)-\tilde{\phi}'(s_1+i\omega_0)}{s_1+i\omega_0-s_3+i\omega_0}. \qquad \text{(C1)}
\end{aligned}$$

Numerical inversion of Eq. (C1) to time domain is used for plotting the photon echo signal. For model M Eq. (C1) simplifies to

$$2\tilde{S}_M(s_3,t_2=0,s_1)=\left[\left(1+\frac{\Lambda}{s_3+i\omega_0+\Lambda}\right)\frac{\Lambda}{(s_3+\Lambda)^2+\omega_0^2-\Lambda^2}+\frac{1}{s_3+i\omega_0+\Lambda}\right]\times\left[\left(1+\frac{\Lambda}{s_1-i\omega_0+\Lambda}\right)\frac{\Lambda}{(s_1+\Lambda)^2+\omega_0^2-\Lambda^2}+\frac{1}{s_1-i\omega_0+\Lambda}\right]+\left[\left(1+\frac{\Lambda}{s_3-i\omega_0+\Lambda}\right)\frac{\Lambda}{(s_3+\Lambda)^2+\omega_0^2-\Lambda^2}+\frac{1}{s_3-i\omega_0+\Lambda}\right]\times\left[\left(1+\frac{\Lambda}{s_1+i\omega_0+\Lambda}\right)\frac{\Lambda}{(s_1+\Lambda)^2+\omega_0^2-\Lambda^2}+\frac{1}{s_1+i\omega_0+\Lambda}\right]. \tag{C2}$$

Equations (33) and (34) are obtained by inverting Eq. (C2) to time domain.

APPENDIX D: THE THIRD-ORDER RESPONSE FUNCTION

We apply Eq. (B1) and Eq. (B2) to the third order response function by setting $n=4$, $L^{(2)}=0$, $L^{(1)}=\pm L^{(3)}$. For the first interval we restore Eq. (A1):

$$\hat{\tilde{R}}^{(1)}(s_1)=[1-\hat{\tilde{\Psi}}(s_1-\hat{L}^{(1)})]^{-1}\hat{\tilde{\Psi}}'(s_1-\hat{L}^{(1)}).$$

Straightforward application of Eqs. (25) and (26) gives for the second interval:

$$\hat{\tilde{R}}^{(2)}(s_2,s_1)=[1-\hat{\tilde{\Psi}}(s_2)]^{-1}[\hat{\tilde{\Psi}}'(s_1-\hat{L}^{(1)})-\hat{\tilde{\Psi}}'(s_2)]\frac{1}{s_2-s_1+\hat{L}^{(1)}}+[1-\hat{\tilde{\Psi}}(s_2)]^{-1}[\hat{\tilde{\Psi}}(s_2)-\hat{\tilde{\Psi}}(s_1-L^{(1)})]\frac{1}{(s_1-\hat{L}^{(1)}-s_2)}\times[1-\hat{\tilde{\Psi}}(s_1-\hat{L}^{(1)})]^{-1}\hat{\tilde{\Psi}}'(s_1-\hat{L}^{(1)}) \tag{D1}$$

and for the third interval

$$\begin{aligned}\hat{\tilde{R}}^{(3)}(s_3,s_2,s_1)=&[1-\hat{\tilde{\Psi}}(s_3-\hat{L}^{(3)})]^{-1}\left[\hat{\tilde{\Psi}}'(s_3-\hat{L}^{(3)})\frac{1}{(s_2-s_3+\hat{L}^{(3)})(s_1-\hat{L}^{(1)}-s_3+\hat{L}^{(3)})}+\hat{\tilde{\Psi}}'(s_2)\frac{1}{(s_3-\hat{L}^{(3)}-s_2)(s_1-\hat{L}^{(1)}-s_2)}\right.\\&\left.+\hat{\tilde{\Psi}}'(s_1-\hat{L}^{(1)})\frac{1}{(s_2-s_1+\hat{L}^{(1)})(s_3-\hat{L}^{(3)}-s_1+\hat{L}^{(1)})}\right]\\&+[1-\hat{\tilde{\Psi}}(s_3-\hat{L}^{(3)})]^{-1}\left[\hat{\tilde{\Psi}}(s_3-\hat{L}^{(3)})\frac{1}{(s_2-s_3+\hat{L}^{(3)})(s_1-\hat{L}^{(1)}-s_3+\hat{L}^{(3)})}+\hat{\tilde{\Psi}}(s_2)\frac{1}{(s_3-\hat{L}^{(3)}-s_2)(s_1-\hat{L}^{(1)}-s_2)}\right.\\&\left.+\hat{\tilde{\Psi}}(s_1-\hat{L}^{(1)})\frac{1}{(s_2-s_1+\hat{L}^{(1)})(s_3-\hat{L}^{(3)}-s_1+\hat{L}^{(1)})}\right]\times[1-\hat{\tilde{\Psi}}(s_1-\hat{L}^{(1)})]^{-1}\hat{\tilde{\Psi}}'(s_1-\hat{L}^{(1)})+[1-\hat{\tilde{\Psi}}(s_3-\hat{L}^{(3)})]^{-1}\\&\times[\hat{\tilde{\Psi}}(s_3-L^{(3)})-\hat{\tilde{\Psi}}(s_2)]\frac{1}{(s_2-s_3+\hat{L}^{(3)})}[1-\hat{\tilde{\Psi}}(s_2)]^{-1}\times\left\{[\hat{\tilde{\Psi}}'(s_1-\hat{L}^{(1)})-\hat{\tilde{\Psi}}'(s_2)]\frac{1}{s_2-s_1+\hat{L}^{(1)}}\right.\\&\left.+[\hat{\tilde{\Psi}}(s_2)-\hat{\tilde{\Psi}}(s_1-L^{(1)})]\frac{1}{(s_1-\hat{L}^{(1)}-s_2)}[1-\hat{\tilde{\Psi}}(s_1-\hat{L}^{(1)})]^{-1}\hat{\tilde{\Psi}}'(s_1-\hat{L}^{(1)})\right\}.\end{aligned} \tag{D2}$$

The Green function Eq. (D3) is obtained by substituting Eqs. (A1), (D1), and (D2) into Eq. (B3). The Green function is given by a sum of 8 terms:

$$\hat{\tilde{G}}^{(3)}(s_3,s_2,s_1)=\sum_{j=1}^{8}\hat{\tilde{G}}_j(s_3,s_2,s_1).$$

Each represents one type of path in the bath space, which is characterized by the presence or absence of any jump in a particular time interval as shown in Fig. 10

$$\hat{\tilde{G}}_1=\hat{\tilde{\Phi}}(s_3-\hat{L}^{(3)})[1-\hat{\tilde{\Psi}}(s_3-\hat{L}^{(3)})]^{-1}[\hat{\tilde{\Psi}}(s_3-L^{(3)})-\hat{\tilde{\Psi}}(s_2)]\times\frac{1}{(s_2-s_3+\hat{L}^{(3)})}[1-\hat{\tilde{\Psi}}(s_2)]^{-1}\times[\hat{\tilde{\Psi}}(s_2)-\hat{\tilde{\Psi}}(s_1-L^{(1)})]\times\frac{1}{(s_1-\hat{L}^{(1)}-s_2)}[1-\hat{\tilde{\Psi}}(s_1-\hat{L}^{(1)})]^{-1}\hat{\tilde{\Psi}}'(s_1-\hat{L}^{(1)}),$$

$$\hat{\tilde{G}}_2 = \hat{\tilde{\Phi}}(s_3 - \hat{L}^{(3)})[1 - \hat{\tilde{\Psi}}(s_3 - \hat{L}^{(3)})]^{-1}[\hat{\tilde{\Psi}}(s_3 - L^{(3)}) - \hat{\tilde{\Psi}}(s_2)] \times \frac{1}{(s_2 - s_3 + \hat{L}^{(3)})}[1 - \hat{\tilde{\Psi}}(s_2)]^{-1}[\hat{\tilde{\Psi}}'(s_1 - \hat{L}^{(1)}) - \hat{\tilde{\Psi}}'(s_2)] \times \frac{1}{s_2 - s_1 + \hat{L}^{(1)}},$$

$$\hat{\tilde{G}}_3 = \hat{\tilde{\Phi}}(s_3 - \hat{L}^{(3)})[1 - \hat{\tilde{\Psi}}(s_3 - \hat{L}^{(3)})]^{-1}\Bigg[\hat{\tilde{\Psi}}(s_3 - \hat{L}^{(3)}) \times \frac{1}{(s_2 - s_3 + \hat{L}^{(3)})(s_1 - \hat{L}^{(1)} - s_3 + \hat{L}^{(3)})} + \hat{\tilde{\Psi}}(s_2) \times \frac{1}{(s_3 - \hat{L}^{(3)} - s_2)(s_1 - \hat{L}^{(1)} - s_2)} + \hat{\tilde{\Psi}}(s_1 - \hat{L}^{(1)}) \frac{1}{(s_2 - s_1 + \hat{L}^{(1)})(s_3 - \hat{L}^{(3)} - s_1 + \hat{L}^{(1)})}\Bigg] \times [1 - \hat{\tilde{\Psi}}(s_1 - \hat{L}^{(1)})]^{-1}\hat{\tilde{\Psi}}'(s_1 - \hat{L}^{(1)}),$$

$$\hat{\tilde{G}}_4 = \hat{\tilde{\Phi}}(s_3 - \hat{L}^{(3)})[1 - \hat{\tilde{\Psi}}(s_3 - \hat{L}^{(3)})]^{-1}\Bigg[\hat{\tilde{\Psi}}'(s_3 - \hat{L}^{(3)}) \times \frac{1}{(s_2 - s_3 + \hat{L}^{(3)})(s_1 - \hat{L}^{(1)} - s_3 + \hat{L}^{(3)})} + \hat{\tilde{\Psi}}'(s_2) \frac{1}{(s_3 - \hat{L}^{(3)} - s_2)(s_1 - \hat{L}^{(1)} - s_2)} + \hat{\tilde{\Psi}}'(s_1 - \hat{L}^{(1)}) \frac{1}{(s_2 - s_1 + \hat{L}^{(1)})(s_3 - \hat{L}^{(3)} - s_1 + \hat{L}^{(1)})}\Bigg],$$

$$\hat{\tilde{G}}_5 = [\hat{\tilde{\Phi}}(s_3 - \hat{L}^{(3)}) - \hat{\tilde{\Phi}}(s_2)] \frac{1}{s_2 - s_3 + \hat{L}^{(3)}}[1 - \hat{\tilde{\Psi}}(s_2)]^{-1} \times [\hat{\tilde{\Psi}}(s_2) - \hat{\tilde{\Psi}}(s_1 - L^{(1)})] \frac{1}{(s_1 - \hat{L}^{(1)} - s_2)} \times [1 - \hat{\tilde{\Psi}}(s_1 - \hat{L}^{(1)})]^{-1}\hat{\tilde{\Psi}}'(s_1 - \hat{L}^{(1)}),$$

$$\hat{\tilde{G}}_6 = [\hat{\tilde{\Phi}}(s_3 - \hat{L}^{(3)}) - \hat{\tilde{\Phi}}(s_2)] \frac{1}{s_2 - s_3 + \hat{L}^{(3)}}[1 - \hat{\tilde{\Psi}}(s_2)]^{-1} \times [\hat{\tilde{\Psi}}'(s_1 - \hat{L}^{(1)}) - \hat{\tilde{\Psi}}'(s_2)] \frac{1}{s_2 - s_1 + \hat{L}^{(1)}},$$

$$\hat{\tilde{G}}_7 = \Bigg[\hat{\tilde{\Phi}}(s_3 - \hat{L}^{(3)}) \frac{1}{s_2 - s_3 + \hat{L}^{(3)}} \frac{1}{s_1 - \hat{L}^{(1)} - s_3 + \hat{L}^{(3)}} + \hat{\tilde{\Phi}}(s_2) \frac{1}{s_3 - \hat{L}^{(3)} - s_2} \frac{1}{s_1 - \hat{L}^{(1)} - s_2} + \hat{\tilde{\Phi}}(s_1 - \hat{L}^{(1)}) \frac{1}{s_3 - \hat{L}^{(3)} - s_1 + \hat{L}^{(1)}} \frac{1}{s_2 - s_1 + \hat{L}^{(1)}}\Bigg][1 - \hat{\tilde{\Psi}}(s_1 - \hat{L}^{(1)})]^{-1}\hat{\tilde{\Psi}}'(s_1 - \hat{L}^{(1)}),$$

$$\hat{\tilde{G}}_8 = \hat{\tilde{\Phi}}'(s_3 - \hat{L}^{(3)}) \frac{1}{s_2 - s_3 + \hat{L}^{(3)}} \frac{1}{s_1 - \hat{L}^{(1)} - s_3 + \hat{L}^{(3)}} + \hat{\tilde{\Phi}}'(s_2) \frac{1}{s_3 - \hat{L}^{(3)} - s_2} \frac{1}{s_1 - \hat{L}^{(1)} - s_2} + \hat{\tilde{\Phi}}'(s_1 - \hat{L}^{(1)}) \frac{1}{s_3 - \hat{L}^{(3)} - s_1 + \hat{L}^{(1)}} \frac{1}{s_2 - s_1 + \hat{L}^{(1)}}. \tag{D3}$$

All necessary matrices $\hat{\tilde{\Phi}}(s - \hat{L})$, $\hat{\tilde{\Psi}}(s - \hat{L})$, and $[1 - \hat{\Psi}(s - \hat{L})]^{-1}$ are readily calculated in Appendix A.

[1] R. Kubo, J. Math. Phys. **4**, 174 (1963).

[2] R. Kubo, in *Flucutation, Relaxation and Resonance in Magnetic Systems*, edited by D. ter Haar (Oliver & Boyd, Edinburgh, 1962), p. 23.

[3] P. W. Anderson, B. I. Halperin, and C. M. Varma, Philos. Mag. **25**, 1 (1971).

[4] G. E. Uhlenbeck and L. S. Ornstein, Phys. Rev. **36**, 823 (1930).

[5] H. Risken, *The Fokker-Plank Equation* (Springer, Berlin, 1989).

[6] A. O. Caldeira and A. Leggett, Physica A **121**, 587 (1983).

[7] R. Zwanzig, in *Lectures in Theoretical Physics*, edited by W. E. Brittin, B. W. Downs, and J. Downs (Interscience, New York, 1961), Vol. III, p. 106.

[8] H. Mori, Prog. Theor. Phys. **33**, 423 (1965).

[9] M. Tokuyama and H. Mori, Prog. Theor. Phys. **55**, 411 (1976).

[10] R. Metzler, E. Barkai, and J. Klafter, Phys. Rev. Lett. **82**, 3563 (1999).
[11] R. Metzler and J. Klafter, Phys. Rep. **339**, 1 (2000).
[12] H. P. Breuer and F. Petruccione, *The Theory of Open Quantum Systems* (Oxford University Press, New York, 2002).
[13] S. C. Kou and X. S. Xie, Phys. Rev. Lett. **93**, 180603 (2004).
[14] W. Min, G. Luo, B. J. Cherayil, S. C. Kou, and X. S. Xie, Phys. Rev. Lett. **94**, 198302 (2005).
[15] S. Mukamel, *Principles of Nonlinear Optical Spectroscopy* (Oxford University Press, New York, 1995).
[16] R. J. Glauber, in *Quantum Optics and Electronics*, edited by C. De Witt, A. Blandin, and C. Cohen-Tannoudji (Gordon and Breach, New York, 1965), p. 65.
[17] V. Barsegov and S. Mukamel, J. Phys. Chem. A **108**, 15 (2004).
[18] F. Šanda and S. Mukamel, Phys. Rev. E **72**, 031108 (2005).
[19] H. Yang, G. Luo, P. Karnchanaphanurach, T-M. Louie, I. Rech, S. Cova, L. Xun, and X. S. Xie, Science **302**, 262 (2003).
[20] O. Flomenbom, K. Velonia, D. Loos, S. Masuo, M. Cotlet, Y. Engelborghs, J. Hofkens, A. E. Rowan, R. J. M. Nolte, F. C. de Schryver, and J. Klafter, Proc. Natl. Acad. Sci. U.S.A. **102**, 2368 (2005).
[21] L. Edman, Z. Földes-Papp, S. Wennmalm, and R. Rigler, Chem. Phys. **247**, 11 (1999).
[22] M. Kuno, D. P. Fromm, H. F. Hamman, A. Gallagher, and D. J. Nesbitt, J. Chem. Phys. **112**, 3117 (2000).
[23] K. T. Shimizu, R. G. Neuhauser, C. A. Leatherdale, S. A. Empedocles, W. K. Woo, and M. G. Bawendi, Phys. Rev. B **63**, 205316 (2001).
[24] G. Messin, J. P. Hermier, E. Giacobino, P. Desbioles, and M. Dahan, Opt. Lett. **26**, 1891 (2001).
[25] W. E. Montroll and G. H. Weiss, J. Math. Phys. **6**, 167 (1965).
[26] H. Scher and M. Lax, Phys. Rev. B **7**, 4491 (1973).
[27] J. W. Haus and K. W. Kehr, Phys. Rep. **150**, 263 (1987).
[28] B. B. Mandelbrot, *The Fractal Geometry of Nature* (Freeman, San Francisco, 1983).
[29] H. Sher and W. E. Montroll, Phys. Rev. B **12**, 2455 (1975).
[30] G. Zumofen, A. Blumen, and J. Klafter, Phys. Rev. A **41**, R4558 (1990).
[31] G. H. Weiss, *Aspects and Applications of the Random Walks* (North-Holland, Amsterdam, 1994).
[32] M. F. Shlesinger, Annu. Rev. Phys. Chem. **39**, 269 (1988).
[33] J. P. Bouchard and A. Georges, Phys. Rep. **195**, 127 (1990).
[34] F. Bardou, J. P. Bouchard, A. Aspect, and C. Cohen-Tannoudji, *Lévy Statistics and Laser Cooling: How Rare Events Bring Atoms to Rest* (Cambridge University Press, Cambridge, UK, 2002).
[35] E. Gudowska-Nowak and K. Weron, Phys. Rev. E **65**, 011103 (2001).
[36] J. Kotulski, J. Stat. Phys. **81**, 777 (1995).
[37] M. F. Shlesinger, J. Stat. Phys. **10**, 421 (1974).
[38] B. V. Gnedenko and A. N. Kolmogorov, *Limit Distributions for Sums of Independent Random Variables* (Addison-Wesley, Reading, MA, 1954).
[39] A. Gut, *Stopped Random Walks Limit Theorems and Applications* (Springer, New York, 1988).
[40] M. M. Meerschaert and H. Scheffler, *Limit Theorems for Sum of Independent Vectors; Heavy Tails in Theory and Practice* (Wiley, New York, 2001).
[41] A. Jurlewicz, Dissertationes Mathematicae **431**, 1 (2005).
[42] G. Bel and E. Barkai, Phys. Rev. Lett. **94**, 240602 (2005).
[43] W. Feller, *An Introduction to Probability Theory and its Application* (Willey, New York, 1971).
[44] R. Verberk and M. Orrit, J. Chem. Phys. **119**, 2214 (2003).
[45] Y. Jung, E. Barkai, and R. Silbey, Chem. Phys. **284**, 181 (2002).
[46] A. I. Shushin, Phys. Rev. E **67**, 061107 (2003).
[47] A. I. Shushin, Physica A **340**, 283 (2004).
[48] A. I. Shushin, cond-mat/0409578, 2004.
[49] M. O. Vlad, V. T. Popa, and E. Segal, Phys. Lett. **100**, 387 (1984).
[50] M. O. Vlad and A. Pop, Physica A **155**, 276 (1989).
[51] C. Cohen-Tanoudji, J. Dupon-Roc, and G. Gryndberg, *Atom Photon Interaction* (Wiley, New York, 1957).
[52] D. R. Cox, *Renewal Theory* (Methuen, London, 1962).
[53] Y. Jung, E. Barkai, and R. Silbey, Adv. Chem. Phys. **123**, 199 (2002).
[54] F. Šanda and S. Mukamel, Phys. Rev. A **71**, 033807 (2005).
[55] G. Margolin and E. Barkai, Phys. Rev. Lett. **94**, 080601 (2005).